Stem Cell Reports

Article

iPSC-MSCs with High Intrinsic MIRO1 and Sensitivity to TNF-α Yield Efficacious Mitochondrial Transfer to Rescue Anthracycline-Induced Cardiomyopathy

Yuelin Zhang,[1] Zhendong Yu,[2] Dan Jiang,[3] Xiaoting Liang,[1] Songyan Liao,[1] Zhao Zhang,[3] Wensheng Yue,[1] Xiang Li,[1] Sin-Ming Chiu,[1] Yuet-Hung Chai,[1,4] Yingmin Liang,[1] Yenyen Chow,[1] Shuo Han,[3] Aimin Xu,[1,4] Hung-Fat Tse,[1,4,5,*] and Qizhou Lian[1,3,4,6,*]

[1]Cardiology Division, Department of Medicine, The University of Hong Kong, Hong Kong, China
[2]Central Laboratory, Peking University Shenzhen Hospital, Shenzhen 518000, China
[3]Department of Ophthalmology
[4]Research Centre of Heart, Brain, Hormone, and Healthy Aging
[5]Hong Kong-Guangdong Joint Laboratory on Stem Cell and Regenerative Medicine, Guangzhou Institutes of Biomedicine and Health
The University of Hong Kong, Hong Kong, China
[6]Shenzhen Institutes of Research and Innovation, The University of Hong Kong, Shenzhen 518000, China
*Correspondence: hftse@hku.hk (H.-F.T.), qzlian@hku.hk (Q.L.)
http://dx.doi.org/10.1016/j.stemcr.2016.08.009

SUMMARY

Mesenchymal stem cells (MSCs) can donate mitochondria and rescue anthracycline-induced cardiomyocyte (CM) damage, although the underlying mechanisms remain elusive. We determined that the superior efficiency of mitochondrial transfer by human induced-pluripotent-stem-cell-derived MSCs (iPSC-MSCs) compared with bone marrow-derived MSCs (BM-MSCs) is due to high expression of intrinsic Rho GTPase 1 (MIRO1). Further, due to a higher level of TNFαIP2 expression, iPSC-MSCs are more responsive to tumor necrosis factor alpha (TNF-α)-induced tunneling nanotube (TNT) formation for mitochondrial transfer to CMs, which is regulated via the TNF-α/NF-κB/TNFαIP2 signaling pathway. Inhibition of TNFαIP2 or MIRO1 in iPSC-MSCs reduced the efficiency of mitochondrial transfer and decreased CMs protection. Compared with BM-MSCs, transplantation of iPSC-MSCs into a mouse model of anthracycline-induced cardiomyopathy resulted in more human mitochondrial retention and bioenergetic preservation in heart tissue. Efficacious transfer of mitochondria from iPSC-MSCs to CMs, due to higher MIRO1 expression and responsiveness to TNF-α-induced nanotube formation, effectively attenuates anthracycline-induced CM damage.

INTRODUCTION

Anthracycline antibiotics, including doxorubicin (Dox), remain the cornerstone of treatment for a variety of malignancies (Arcamone et al., 2000). Nonetheless, they are well known to cause dose-dependent, progressive myocardial damage known as anthracycline-induced cardiomyopathy (AIC), which hinders their broad clinical application (Chen et al., 2011). As more cancer patients survive, AIC has become more prevalent and is now the leading cause of morbidity and mortality among such patients. Although there remains some controversy about the conflicting beneficial (anticancer) and detrimental (cardiotoxic) effects of anthracycline therapy, compelling evidence indicates that different mechanisms are involved. Of note, anthracycline antitumor efficacy is associated with nuclear DNA intercalation topoisomerase II inhibition and drug-DNA adduct formation (Capranico et al., 1989). Cardiotoxicity is largely ascribed to oxidative stress and mitochondrial damage (Lebrecht et al., 2005). Recent studies suggest that inhibition of mitochondrial biogenesis is the main pathology underlying AIC (Suliman et al., 2007) and is separate from its antineoplastic activity of topoisomerase II inhibition (Holm et al., 1989). Although angiotensin-converting enzyme inhibitors alone or with β-blockers may limit the progression of AIC (Georgakopoulos et al., 2010), the only curative therapy for those with severe heart failure is heart transplantation (Lenneman et al., 2013).

Anthracycline-induced inflammation and mitochondrial damage can lead to disruption of the homeostasis of endogenous myocardial regeneration by direct cardiomyocyte (CM) death and depletion of resident cardiac progenitor cells (De Angelis et al., 2010). It has been shown that transplantation of adult mesenchymal stem cells (MSCs) protects CMs against AIC (Pinarli et al., 2013), but the underlying mechanisms remain unclear. They may be related to large variations in MSCs derived from different sources (Xin et al., 2010). Compared with adult MSCs, single-cell colony-derived MSC lines from human pluripotent stem cells (PSCs) show the same phenotype as bone marrow (BM)-MSCs and exhibit tissue repair (Lian et al., 2010) and anti-inflammatory (Sun et al., 2015) actions. In addition, they have the advantage of less batch-to-batch variation and can be expanded to >120 population doublings without obvious senescence (Lian et al., 2010). Apart from the secretion of paracrine factors (Amsalem et al., 2007), recent studies also report efficacious direct mitochondrial transfer from induced PSC-derived MSCs

(iPSC-MSCs) to injured cells as another mechanism to protect against tissue injury (Islam et al., 2012; Li et al., 2014). Based on these observations and the fact that iPSC-MSCs display a much higher efficiency for mitochondria transfer than adult BM-MSCs in response to inflammation, we hypothesized that this higher mitochondrial transfer potential may be associated with some intrinsic molecules involved in mediating mitochondrial movement to the native cells after transplantation. In this study, we have revealed that functional mitochondrial transfer from human iPSC-MSCs plays a critical role in cardio-protection against Dox-induced mitochondrial damage. Importantly, we demonstrated that the higher efficiency of mitochondrial transfer from human iPSC-MSCs is attributed to high-level intrinsic expression of MIRO1, a mitochondrial Rho GTPase 1 that can modulate intercellular mitochondrial movement along microtubules (Ahmad et al., 2014). Moreover, iPSC-MSCs were more responsive than BM-MSCs to pro-inflammatory cytokine tumor necrosis factor alpha (TNF-α)-induced formation of tunneling nanotubes (TNT) (Wang et al., 2011), through which mitochondria were transported.

RESULTS

Efficiency of Mitochondrial Transfer from iPSC-MSCs to CMs in Response to Dox-Induced Injury

We first examined the mitochondrial transfer from MSCs to neonatal mice CMs (NMCs) under Dox challenge. Co-culture of Celltrace-labeled NMCs (violet) and MitoTracker-labeled MSCs (green) revealed mitochondrial transfer from MSCs to NMCs (Figures S1Ai–S1Aiv). In agreement with previous studies (Ahmad et al., 2014; Vallabhaneni et al., 2012), in the co-culture of NMCs and MSCs, we detected only MitoTracker of MSCs in NMCs but no Celltrace of NMCs in MSCs. Co-culture of human MSCs with NMCs indicated that human mitochondrial COX-4 was detected in NMCs that were positive for TROPONIN expression (Figures S1Bv –S1Bvii). We further examined the mitochondrial transfer efficiency after 4, 12, 24, and 48 hr of co-culture. Compared with BM-MSCs, more effective mitochondrial transfer from iPSC-MSCs to NMCs was detected by fluorescence-activated cell sorting (FACS) after 24 and 48 hr co-culture (Figures 1Ai and 1Aii). Moreover, the mitochondrial transfer ratio of MSCs to NMCs at 48 hr was similar to that at 24 hr, indicating that 24 hr co-culture of MSCs with NMCs achieved the peak efficiency of mitochondrial transfer with and without Dox challenge. Notably, mitochondrial uptake was enhanced when NMCs were exposed to Dox, suggesting that injured NMCs increased the uptake of mitochondria from iPSC-MSCs (Figure 1Aii). We also examined the mitochondrial

transfer efficiency from iPSC-MSCs to adult mice HL-1 or human AC16 CMs. Compared with NMCs, no significant difference in mitochondrial transfer ratio was observed from iPSC-MSCs to either HL-1 or AC16 CMs (Figure S1C), indicating that the efficiency of mitochondrial transfer from MSCs to CMs is not determined by the stage of CMs, but more likely the conditions to which they are exposed.

To exclude the possibility of leakage of MitoTracker green dye taken up by NMCs from medium, we transfected iPSC-MSCs with a lentiviral-mediated mitochondrial-specific fragment fused with GFP (LV-MITO-GFP), allowing us to monitor mitochondrial trafficking. MITO-GFP-iPSC-MSCs (Figure 1Bi) were co-cultured with NMCs for 24 hr under Dox challenge. Immunostaining showed that TROPONIN-positive NMCs were positive for MITO-GFP, indicating that mitochondria had translocated from MSCs to NMCs (Figures 1Bii–1Biv). We also co-cultured unlabeled NMCs with pLL3.7-GFP lentivirus-labeled iPSC-MSCs under Dox for 24 hr. Unlabeled NMCs were separated from the co-culture. Isolated NMCs were subjected to immunostaining for anti-TROPONIN and anti-human mitochondrial COX-4. We observed the presence of human COX-4 in NMCs, indicating that mitochondrial transfer had occurred between iPSC-MSCs and NMCs (Figures 1Ci–1Ciii).

Functional Mitochondrial Transfer by iPSC-MSCs Protects against Dox-Induced CM Damage and Is Independent of Paracrine Action of MSCs

We examined whether mitochondria transferred from MSCs to NMCs are functional. Celltrace-labeled NMCs and MITO-GFP-iPSC-MSCs were co-cultured for 24 hr under Dox challenge. Cells were separated by cell sorting (Figure 1Di). To verify the successful separation, immunostaining showed that TROPONIN-positive cells were co-localized with MITO-GFP in mitochondrial-transferred NMCs (Figure 1Dii), and no MITO-GFP was detected in non-mitochondrial-transferred NMCs (Figure 1Diii). To determine the respiratory function of transferred mitochondria, the cellular oxygen consumption rate (OCR) of NMCs with and without transferred mitochondria was examined. The bioenergetics profiles of different groups of NMCs are shown in Figure 1E. Four measurements were made: (1) basal mitochondrial OCR measured in medium containing 4.5 g/L glucose; (2) after inhibition of ATP synthase with oligomycin (Olig) (1 μM), ATP synthesis turnover and respiration driving proton leak were assessed by measuring OCR; (3) after treatment with the uncoupling agent carbonyl cyanide-*p*-trifluoromethoxyphenylhydrazone (FCCP) (2 μM), maximal mitochondrial respiratory capacity was determined by OCR; and (4) non-mitochondrial respiration was assessed by measuring OCR after
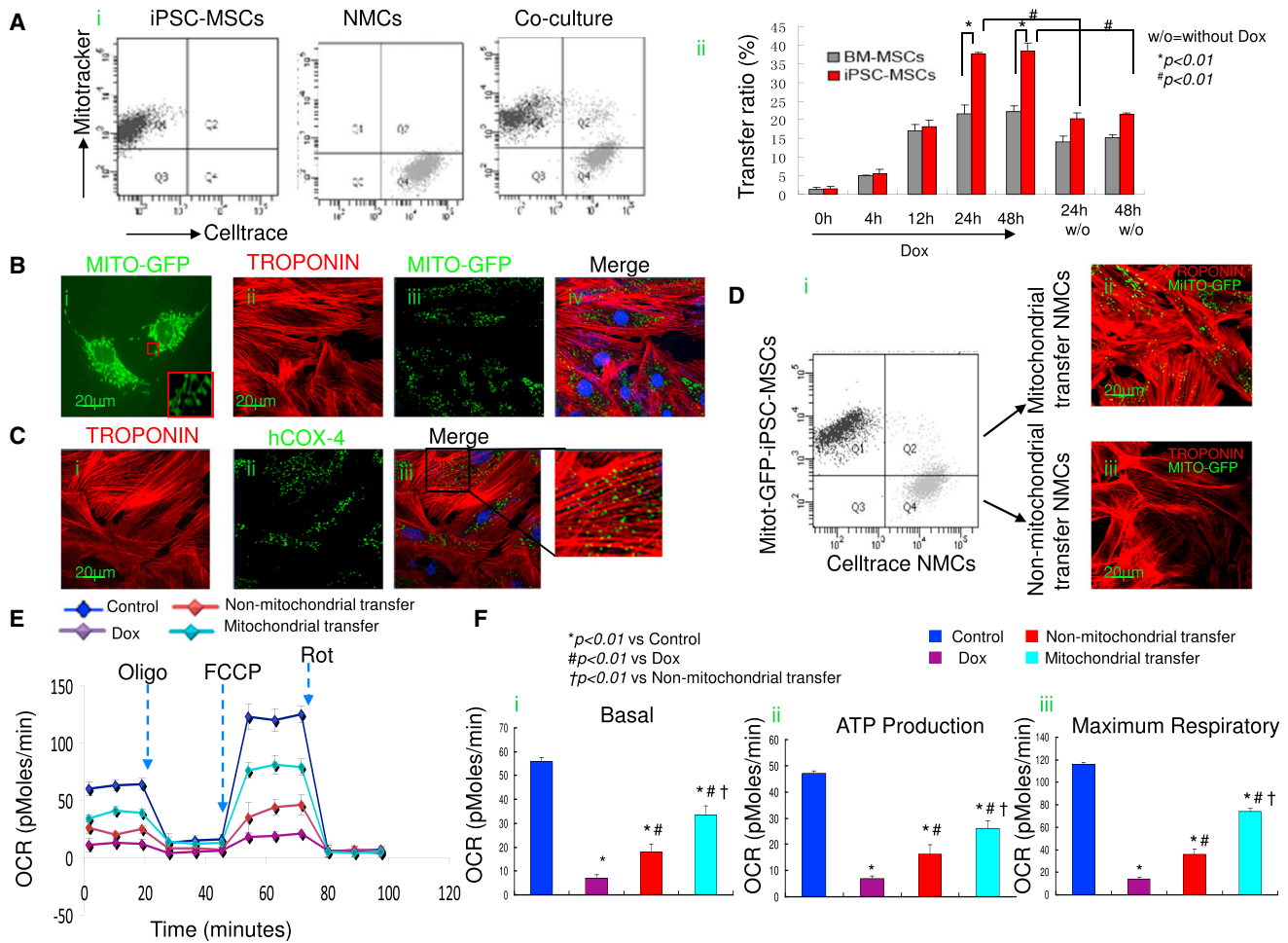
Figure 1. Distinct Mitochondria Transfer from iPSC-MSCs to NMCs Rescues Dox-Induced Mitochondrial Damage and Preserves Cellular Bioenergetics

(A) (Ai) Representative distribution of Celltrace-labeled NMCs (violet) and MitoTracker-labeled MSCs (green) in co-cultured cells analyzed by FACS. (Aii) Time course of the mitochondrial transfer ratio between MSCs and Dox-stressed NMCs distributed at Q2 phase and the percentage of this population over the total NMCs are presented (*p < 0.01, iPSC-MSCs vs BM-MSCs; #p < 0.01, non-Dox stressed versus Dox stressed).

(B) (Bi) iPSC-MSCs were transfected with lentiviral-MITO-GFP plasmid. (Bii, Biii, and Biv) MITO-GFP-MSCs were co-cultured with Celltrace-labeled NMCs under Dox challenge for 24 hr. After sorting, immunostaining showed that MITO-GFP was present in NMCs, indicating transfer of MITO-GFP from MSCs to NMCs (Biv).

(C) Co-culturing of NMCs with pLL3.7-GFP lentivirus-iPSC-MSCs for 24 hr, and sorting out GFP-negative NMCs. Immunostaining of TROPONIN and human COX-4 in the NMCs revealed the presence of human mitochondria (Ci–Ciii).

(D) After co-culture, the mitochondrial-transferred and the non-mitochondrial-transferred NMCs were separated by FACS (Di). Representative images illustrating MITO-GFP expression in mitochondrial-transferred NMCs (Dii) but not in non-mitochondrial-transferred NMCs (Diii).

(E) OCR of NMCs from different groups was measured over time (minutes). The injection order of Olig, FCCP, and Rot are shown.

(F) Basal mitochondrial OCR (Fi), ATP production (Fii), and maximum respiration (Fiii) of NMCs from different groups was calculated (*p < 0.01 versus control; #p < 0.01 versus Dox; †p < 0.01 versus non-mitochondrial transfer).

Data represent the means ± SD of three independent experiments.

treatment with complex I inhibitor, rotenone (Rot) (2 μM). Compared with control NMCs, basal mitochondrial OCR, ATP production, and maximum respiration were significantly decreased in the Dox-treated NMCs but greatly recovered in NMCs isolated after co-culture with iPSC-MSCs (Figure 1F). Basal mitochondrial OCR, ATP production, and maximum mitochondrial respiratory function were markedly improved in NMCs with mitochondria

transferred from MSCs compared with NMCs without transferred mitochondria (Figure 1F).

We also tested the effect of mitochondrial transfer of MSCs on the viability of NMCs exposed to Dox challenge for 24 hr. Compared with control NMCs, Dox-induced necrosis of NMCs was dramatically attenuated after co-culture with MSCs (Figures S2A and S2B). Notably, using the same NMC and MSC co-culture system, after we separated mitochondrial-transferred NMCs from non-mitochondrial-transferred NMCs, cell death was far less for NMCs with transferred mitochondria, indicating that mitochondrial transfer from MSCs was protective against Dox, and such protection was independent of the paracrine action of iPSC-MSCs (Figures S2A and S2B). In addition, MSCs were less sensitive than CMs to Dox-induced cell death: 1 μM Dox treatment notably damaged NMCs (Figures S2A and S2B), whereas MSCs were not obviously affected (Figure S2C).

To further clarify that functional improvement was due to the transferred mitochondria, we compared the mitochondrial respiratory function of NMCs with transferred mitochondria, purified from either native iPSC-MSCs or Rot-treated iPSC-MSC co-culture. Rot has been used to induce mitochondrial dysfunction (Ahmad et al., 2014). Compared with control NMCs, mitochondrial OCR of NMCs was notably reduced after treatment with 50 nM Rot for 2 hr, although viability of NMCs was not affected (data not shown). Therefore, MITO-GFP-iPSC-MSCs were treated with PBS or Rot for 2 hr and then co-cultured with Celltrace-labeled NMCs for 24 hr under Dox challenge. FACS analysis showed that the efficiency of mitochondrial transfer from Rot-treated and non-Rot-treated iPSC-MSCs to NMCs was similar (data not shown). Next, NMCs with transferred mitochondria were isolated from iPSC-MSCs or Rot-treated iPSC-MSCs, and OCR was measured. The bioenergetics profile of different groups is shown in Figure 2A. Compared with only Dox-treated NMCs, Dox-treated NMCs isolated from co-culture with iPSC-MSCs or Rot-treated iPSC-MSCs presented markedly higher levels of basal mitochondrial OCR, ATP production, and maximum mitochondrial respiratory function (Figures 2Bi–2Biii). Notably, compared with NMCs isolated from Rot-treated MSCs, NMCs isolated from iPSC-MSCs further showed a significantly higher level of basal mitochondrial OCR, ATP production, and maximum respiratory mitochondrial function, highlighting that only functional mitochondrial transfer could strongly protect NMCs. Those MSCs with impaired mitochondria (i.e., aged MSCs) may not be acceptable therapeutic donors. We also examined cytokines secreted by iPSC-MSCs and Rot-treated iPSC-MSCs with or without TNF-α stimulation. There was no significant difference between MSCs and Rot-treated MSCs in the secretion of monocyte chemotactic protein-1 (MCP-1), interleukin-6 (IL-6), and interleukin-8 (IL-8), or vascular endothelial growth factor (VEGF), both in basal conditions and when stimulated by TNF-α (Figures 2Ci–2Civ), suggesting that the functional protection afforded to NMCs by mitochondrial transfer is separate to the above paracrine effect.

iPSC-MSCs with High Potency of Mitochondrial Transfer Have High Expression of Intrinsic MIRO1

To explore the molecular basis of the higher efficiency of mitochondrial transfer by PSC-derived MSCs compared with BM-MSCs, we reviewed our previous microarray data (Lian et al., 2007, 2010). Pairwise comparison of gene expression between human embryonic stem cell (hESC)/iPSC-MSCs and BM-MSCs revealed a correlation coefficient of 0.72 (Lian et al., 2007), suggesting significant conservation of gene expression in both hESC-MSCs and BM-MSCs, albeit with a few differences. A search for the distinguishing expression level of mitochondrial motor-protein-related genes among hESC-MSCs, iPSC-MSCs, and BM-MSCs, revealed that MIRO1, an integral protein involved in mitochondrial transportation (Ahmad et al., 2014), is highly expressed by human iPSC-MSCs and hESC-MSCs but not BM-MSCs. Western blot confirmed that the protein level of MIRO1 is truly overpresented in human iPSC-MSCs and hESC-MSCs compared with BM-MSCs (Figures 3Ai and 3Aii).

To determine whether a high level of MIRO1 is a real key driver for the high level of intercellular mitochondrial transfer in iPSC-MSCs, we performed a loss- and gain-of-function experiment by knockdown of MIRO1 with short hairpin RNA (shRNA) and replenishment by overexpression of MIRO1. Accordingly, MITO-GFP-iPSC-MSCs were introduced with scramble control shRNA (iPSC-MSCs-MIRO1^{Sc}), MIRO1-shRNA (iPSC-MSCs-MIRO1^{Lo}) and overexpressed *MIRO1* (iPSC-MSCs-MIRO1^{Hi}), respectively, and co-cultured with Celltrace-labeled NMCs at 1:1 ratio under Dox challenge. After 48 hr, the mitochondrial transfer ratio of MSCs to NMCs was measured by FACS. Compared with scramble shRNA-treated iPSC-MSCs (iPSC-MSCs-MIRO1^{Sc}), the protein level of MIRO1 was remarkably decreased in iPSC-MSCs-MIRO1^{Lo} and was accompanied by a significant reduction in mitochondrial donation (Figures 3Bi–3Biii). Conversely, overexpression of MIRO1 in iPSC-MSCs-MIRO1^{Hi} resulted in a striking increase in mitochondrial donation (Figures 3Bi–3Biii). Similarly, co-culture of BM-MSCs of overexpressed MIRO1 with NMCs under Dox challenge also led to an enhanced mitochondrial transfer efficiency compared with native BM-MSCs (Figures S3A and S3B). These results indicate that MIRO1 is a key molecule governing intercellular mitochondrial movement in iPSC-MSCs. On the contrary, when MIRO1
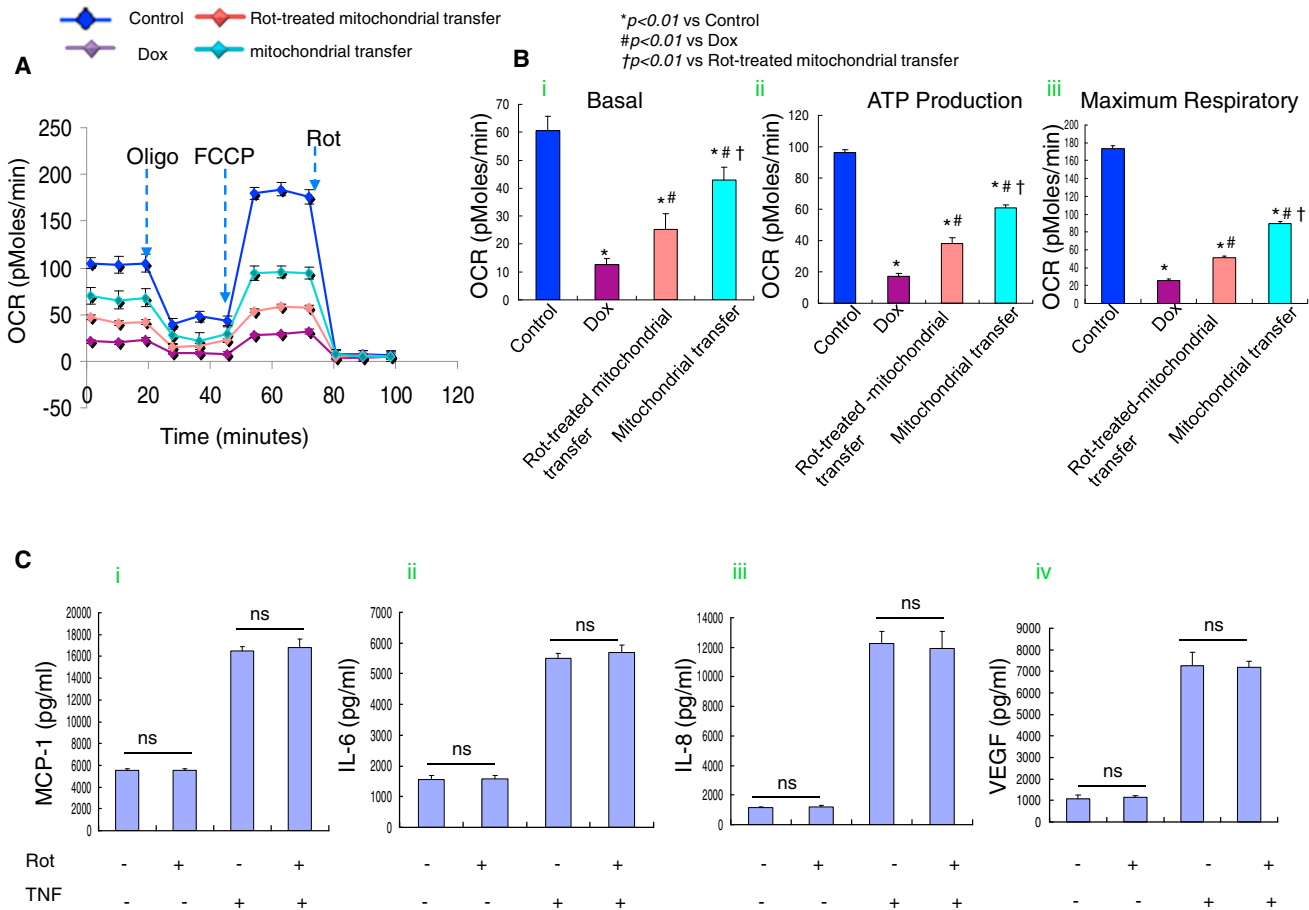
Figure 2. Mitochondrial Transfer from iPSC-MSCs Rescues Dox Insult and Is Independent of Paracrine Effects

(A) OCR of NMCs sorted from Rot-treated iPSC-MSCs or iPSC-MSCs was measured over time (minutes).

(B) Basal mitochondrial OCR (Bi), ATP production (Bii), and maximum respiration (Biii) of NMCs from different groups was calculated.

(C) Quantification of paracrine products including MCP-1 (Ci), IL-6 (Cii), IL-8 (Ciii), and VEGF (Civ) secreted by iPSC-MSCs with or without Rot treatment after TNF-α stimulation.

Data represent the means ± SD of three independent experiments. *p < 0.01 versus control; #p < 0.01 versus Dox; †p < 0.01 versus Rot-treated mitochondrial transfer. NS, not significant.

was overexpressed in NMCs that were then co-cultured with iPSC-MSCs under Dox challenge, the high level of MIRO1 in NMCs had no impact on the mitochondrial transfer from MSCs to NMCs (Figures S3C and S3D). To verify that MITO-GFP translocation indicates real mitochondrial transfer, MITO-GFP positive and negative NMCs were separated. GFP and mitochondrial-component human COX-4 protein were detected in the MITO-GFP+-NMC subpopulation, suggesting that MITO-GFP is a reliable reporter of mitochondrial transfer from MSCs to NMCs (Figures 3Ci–3Ciii). Compared with the NMCs exposed to iPSC-MSCs-MIRO1^{Sc}, inhibition of MIRO1 (iPSC-MSCs-MIRO1^{Lo}) resulted in reduced abundance of MITO-GFP and human COX-4 in the MITO-GFP+-NMCs. Overexpression of MIRO1 (iPSC-MSCs-MIRO1^{Hi}) increased

the abundance of MITO-GFP and human Cox4 content in MITO-GFP+-NMCs (Figures 3Ci–3Ciii).

Formation of TNT between iPSC-MSCs and CMs for Mitochondrial Transfer

It has been reported that F-actin-modulated formation of TNT is a viable mechanism for mitochondrial transfer between adult stem cells and somatic cells and rescues their respiration (Spees et al., 2006; Vallabhaneni et al., 2012). We examined in vitro the role of TNT in the regulation of iPSC-MSC mitochondrial transfer. MITO-GFP-iPSC-MSCs were co-cultured with Celltrace-labeled NMCs under Dox challenge. After 24 hr, staining with rhodamine phalloidin, a high-affinity F-actin probe, showed that NMCs and iPSC-MSCs were bridged by TNT, which allowed effective
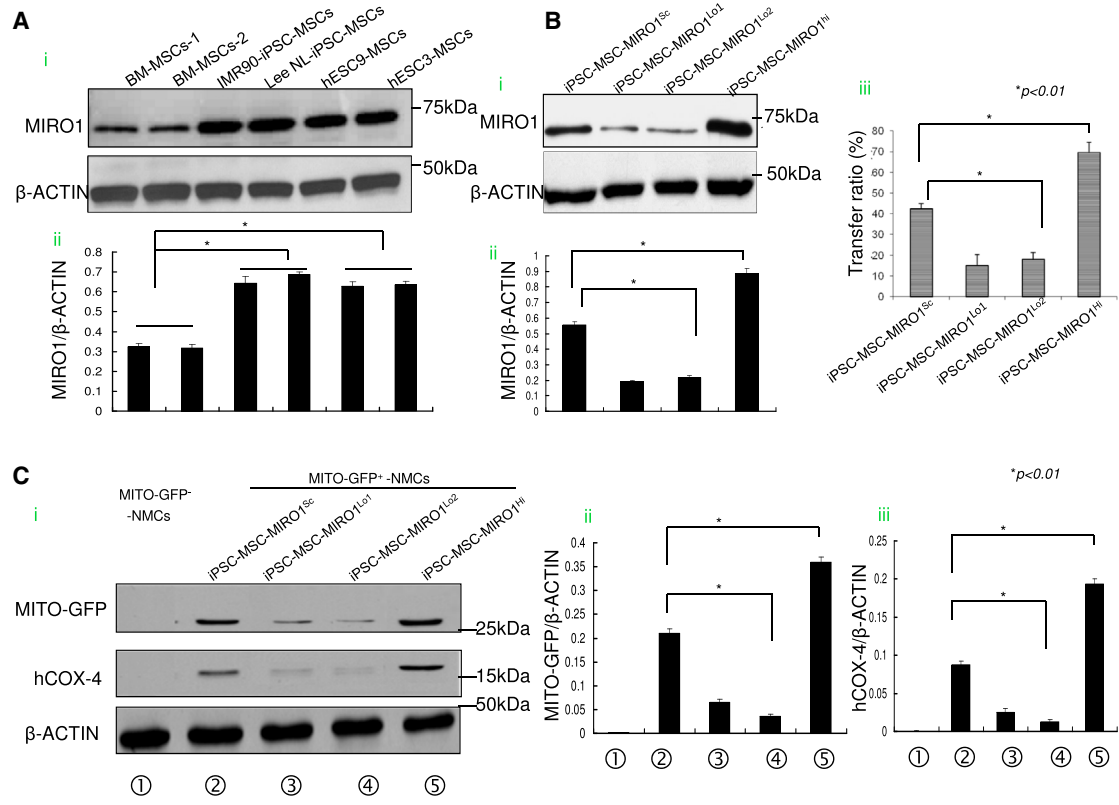
Figure 3. High Expression of Intrinsic MIRO1 by iPSC-MSCs Contributes to Mitochondrial Transfer

(A) The expression of MIRO1 by different types of iPSC-MSCs/ESC-MSCs was detected (Ai and Aii).

(B) (Bi) MIRO1 was measured in iPSC-MSCs transfected with scramble control shRNA (iPSC-MSCs-MIRO1^Sc), MIRO1-shRNA (iPSC-MSCs-MIRO1^Lo), or MIRO1 cDNA plasmid (iPSC-MSCs-MIRO1^Hi). (Bii) The expression of MIRO1 among different groups was evaluated. (Biii) Mitochondrial transfer ratios between GFP-labeled (green) iPSC-MSCs-MIRO1^Sc, iPSC-MSCs-MIRO1^Lo, or iPSC-MSCs-MIRO1^Hi and stressed Celltrace-labeled NMCs (violet) were measured by FACS. We gated out violet+ NMCs and separated them into a violet+/GFP + population with mitochondria transfer (MITO-GFP^+-NMCs) and a violet+/GFP− population without mitochondria transfer (MITO-GFP^−-NMCs) to calculate the transfer ratio (violet+/GFP+ cells divided by the total violet+ cells).

(C) (Ci) Western blot analysis for expression of GFP and human COX-4 in the mitochondrial-transferred NMCs that were isolated after co-culture with iPSC-MSCs-MIRO1^Sc, iPSC-MSCs-MIRO1^Lo, or iPSC-MSCs-MIRO1^Hi. The expression of GFP (Cii) and human COX-4 (Ciii) among the different groups was evaluated.

Data represent the means ± SD of three independent experiments. *p < 0.01.

transfer of iPSC-MSC mitochondria to injured NMCs (Figures 4Ai–4Aiv), suggesting that TNT are vital for mitochondrial transfer. These findings were further confirmed by time-lapse filming, which enabled us to monitor mitochondrial movement via TNT between iPSC-MSCs and NMCs (Movies S1 and S2). We also examined TNT formation between MSCs and heathy NMCs: few TNT formations between MSCs and healthy NMCs were observed compared with MSCs and injured NMCs (data not shown). To determine whether NMCs could take up leaked MSC mitochondria from media without cell-cell connection, we treated cells with cytochalasin B (Figure 4B), which causes F-actin aggregation and retards TNT formation by inhibiting actin polymerization and philiopodia elonga-

tion without affecting endocytosis (Abounit and Zurzolo, 2012; Cho et al., 2012). Administration of cytochalasin B (350 nM) did not affect MSC viability (data not shown) but almost no TNT formation by iPSC-MSCs was observed (Figure 4Biii). Little mitochondrial transfer from MSCs was detected when NMCs were exposed to Dox (Figure 4Biv), and the viability of NMCs was reduced, suggesting that cell-cell contact, such as TNT, is essential for intercellular mitochondrial transfer and to protect NMCs against Dox-induced damage. As expected, the FACS result showed that cytochalasin B treatment significantly reduced mitochondrial transfer from iPSC-MSCs to NMCs (Figure 4C).

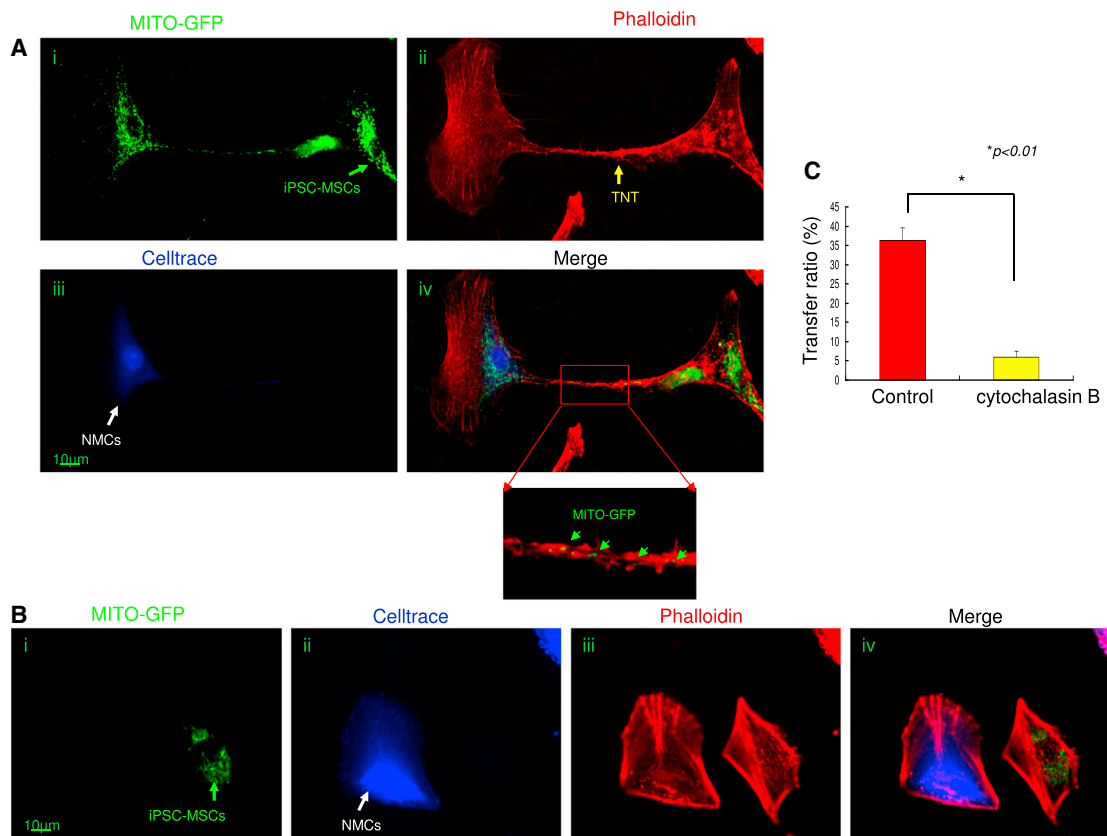To explore whether the mitochondrial transfer is uni- or bidirectional, we co-cultured MITO-GFP-NMCs with

Figure 4. Effective Mitochondrial Transfer from iPSC-MSCs to Rejuvenate NMCs Is Mediated by TNT

(A) Representative images showing TNT formation and mitochondrial transfer between iPSC-MSCs and NMCs. (Ai) MITO-GFP labeling. (Aii) Celltrace labeling. (Aiii) Phalloidin staining showing TNT formation between NMCs and iPSC-MSCs. (Aiv) Representative images of mitochondrial transfer from MSCs to NMCs via TNT. Green arrows show that some MITO-GFP mitochondria were in the middle of the TNT.

(B) Representative image showing that TNT formation and mitochondrial transfer between NMCs and iPSC-MSCs were partially inhibited by pre-treatment of MSCs with cytochalasin B. (Bi) MITO-GFP labeling. (Bii) Celltrace labeling. (Biii) Phalloidin staining showing inhibition of TNT formation between NMCs and iPSC-MSCs. (Biv) Image illustrating the abolition of mitochondrial transfer from MSCs to NMCs.

(C) Mitochondrial transfer ratio between iPSC-MSCs and NMCs under cytochalasin B was analyzed by FACS.

Data represent the means ± SD of three independent experiments. *p < 0.01.

Celltrace-labeled iPSC-MSCs for 24 hr under Dox challenge. Some MITO-GFP that originated from NMCs was detected in iPSC-MSCs although the level of MITO-GFP in iPSC-MSCs was much lower than in NMCs, suggesting that mitochondrial transfer is bidirectional, not unidirectional (Figure S4).

Responsiveness of iPSC-MSCs to TNF-α-Induced Nanotube Formation Is Regulated via the TNF-α/NF-κB/TNFαIP2 Signaling Pathway

Stress conditions or TNF-α can stimulate the formation of TNTs between MSCs (Ahmad et al., 2014; Wang et al., 2011). TNF-α was dramatically increased in mice with AIC (Figure S7Diii) and when NMCs were exposed to Dox challenge (from 360 ± 40 pg/mL to 5,880 ± 380 pg/mL, p < 0.01). TNT formation was increased when MSCs were

exposed to TNF-α (20 ng/mL) (Figure 5Ai). PCR analysis showed that TNF-α-treated MSCs displayed a significantly increased expression of *TNFαIP2*, a TNF-α-induced protein that regulates TNT formation (Figure 5Aii) (Ahmad et al., 2014; Hase et al., 2009). In addition, compared with BM-MSCs, expression of *TNFαIP2* was markedly higher in iPSC-MSCs responsive to TNF-α and was accompanied by a significant increase in TNT numbers per cell (Figure 5Aiii). Nonetheless TNF-α-potentiated TNT formation was largely diminished by small interfering RNA (siRNA)-mediated knockdown of *TNFαIP2* in both BM-MSCs and iPSC-MSCs (Figures 5Ai–5Aiii), indicating that *TNFαIP2* is a downstream protein of TNF-α in the modulation of TNT formation. Depletion of TNF-α from iPSC-MSC medium by TNF-α antibody strikingly decreased the elevated expression of *TNFαIP2* (Figure 5Bi). Similarly, TNF-α-augmented
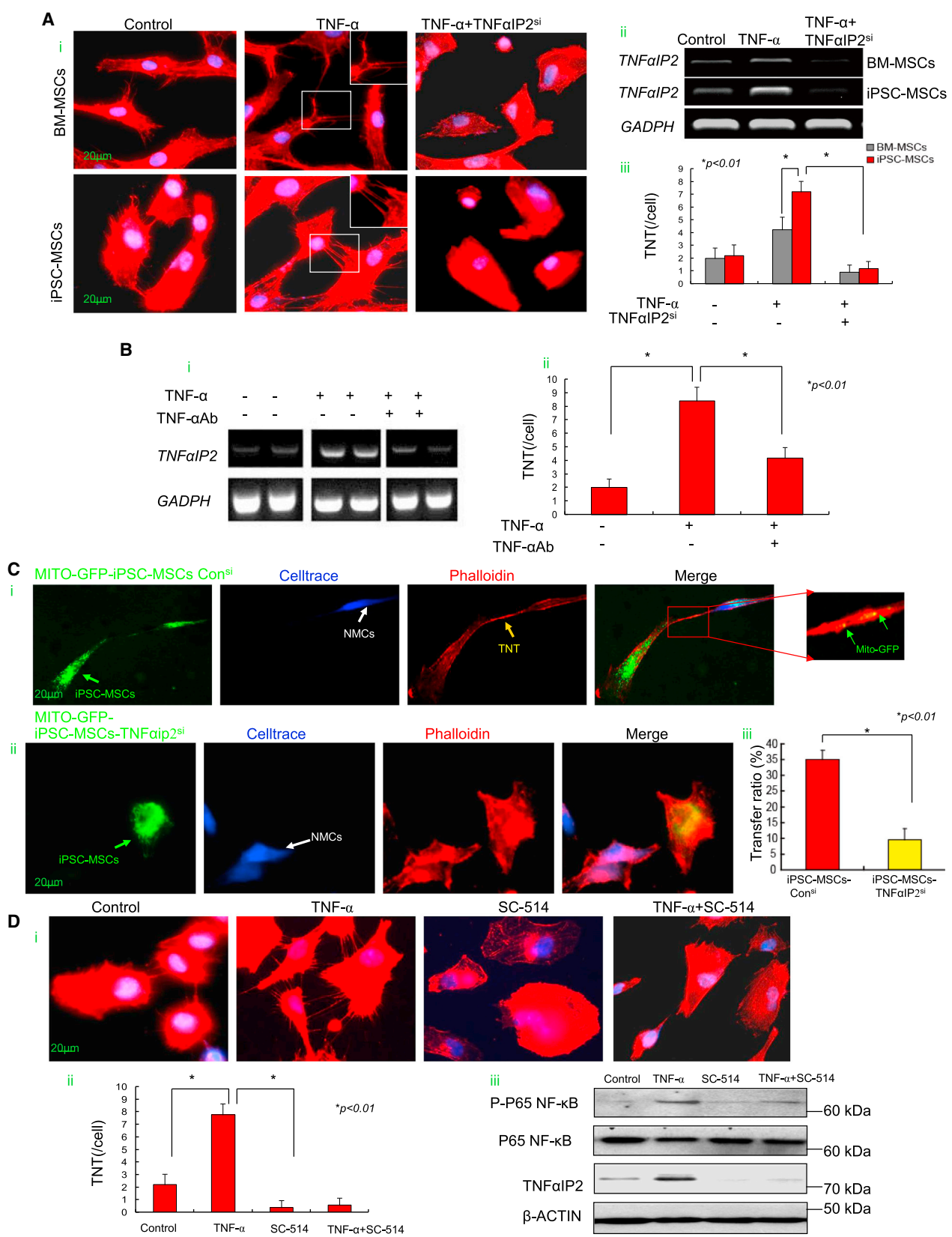
(legend on next page)

TNT formation was largely decreased when TNF-α was depleted with TNF-α antibody in iPSC-MSC culture (Figure 5Bii).

We co-cultured the TNFαIP2siRNA-treated iPSC-MSCs with NMCs and found TNT formation and mitochondrial transfer were abrogated in the TNFαIP2siRNA-treated group (Figures 5Ci and 5Cii). Likewise, FACS analysis showed that after 24 hr co-culture of NMCs with control siRNA or TNFαIP2siRNA-treated iPSC-MSCs under Dox challenge, the mitochondrial transfer ratio in the iPSC-MSCs-TNFαIP2^{si} group was significantly reduced compared with the iPSC-MSCs-con^{si} group (Figure 5Ciii). In contrast, compared with native BM-MSCs, TNT formation and the mitochondrial transfer ratio were significantly increased when BM-MSCs were overexpressed with TNFαIP2 under Dox challenge (Figures S5A–S5C). Further, the mitochondrial transfer ratio in the BM-MSCs-TNFαIP2^{si} group was significantly reduced compared with the BM-MSCs-con^{si} group (Figure S5D).

To determine whether TNFαIP2-induced TNT formation is mediated by the NF-κB pathway, we examined the phosphorylated level of NF-κB subunit P65 (P-P65) and TNT formation in iPSC-MSCs. TNF-α treatment enhanced TNT formation (Figures 5Di and 5Dii), while the level of P-P65 and TNFαIP2 was also significantly increased (Figure 5Diii). In contrast, treatment with NF-κB inhibitor SC-514 (1 μM) significantly attenuated the level of P-P65 and TNFαIP2, and abolished TNF-α-induced TNT formation (Figures 5Di and 5Dii), suggesting that the TNF-α/NF-κB/TNFαIP2 signaling pathway is predominantly involved in TNF-α-mediated TNT formation by MSCs. We also measured the expression of NF-κB and TNFαIP2 in the iPSC-MSCs-MIRO1^{si} and iPSC-MSCs-MIRO1^{Hi}. The expression level of NF-κB activity and TNFαIP2 in both iPSC-MSCs-MIRO1^{si} and iPSC-MSCs-MIRO1^{Hi} was similar to the control iPSC-MSCs, indicating no direct relationship between MIRO1 and NF-κB/TNFαIP2 (data not shown).

Transplantation of iPSC-MSCs but Not TNFαIP2^{si}-Treated iPSC-MSCs Effectively Protects against Dox-Induced Cardiomyopathy

The experimental protocol is outlined in Figure 6A. Heart function was evaluated by echocardiogram and pressure-volume loop study (Figures 6B and 6C). At week 0, administration of Dox significantly decreased the left ventricular (LV) ejection fraction (LVEF) and fractional shortening (FS) compared with the control group, indicating successful establishment of an animal model of Dox-induced cardiomyopathy (Figures 6Bi and 6Bii). At 3 weeks after cell transplantation, LVEF, FS, LV +dp/dt, and LV systolic pressure (LVSP) were significantly improved in the MSC transplantation group compared with the Dox group (Figure 6C). The LVEF, FS, +dp/dt, and LVSP were also significantly higher in the iPSC-MSC group compared with the iPSC-MSCs-TNFαIP2^{si} and BM-MSC groups (Figure 6C). Moreover, LV internal diameter end diastole (LVIDd) was greatly reduced and LV posterior wall end diastole (LVPWd) was significantly increased in the MSC transplantation group compared with the Dox group (Figures S6A and S6B). Notably, there were significant differences in LVIDd and LVPWd in the iPSC-MSCs group compared with iPSC-MSCs-TNFαIP2^{si} and BM-MSCs groups (Figures S6A and S6B).

Histological analysis revealed typical features of Dox-induced cardiotoxicity, including a dilated LV chamber, extensive CM death, myofibrillar degeneration, and vacuolization (Figures 6Di–6Dx). MSC transplantation significantly attenuated LV dilatation and myocardial damage induced by Dox (Figures 6Di–6Dx). Sirius red staining demonstrated a significantly increased extent of myocardial fibrosis in the Dox group compared with control group (Figures 6Dxi–6Dxv and 6E). Nonetheless, 3 weeks after cell

Figure 5. TNF-α Mediates TNT Formation by MSCs through the NF-κB Pathway and Contributes to Mitochondrial Transfer from MSCs to NMCs

(A) (Ai) TNT formation was mediated by TNF-α stimulation and abrogated by TNFαIP2siRNA in iPSC-MSCs and BM-MSCs. (Aii) PCR showing that *TNFαIP2* was significantly increased with TNF-α stimulation and reduced by TNFαIP2siRNA intervention. (Aiii) TNT number of one cell in the iPSC-MSC and BM-MSC groups when exposed to TNF-α or TNFαIP2siRNA intervention was calculated.

(B) (Bi) The elevated *TNFαIP2* expression induced by TNF-α was strikingly decreased in iPSC-MSCs when TNF-α was depleted from the iPSC-MSC culture medium by immunoprecipitation with antibody TNF-α. (Bii) TNF-α-augmented TNT formation was largely decreased when TNF-α was neutralized by TNF-α antibody in iPSC-MSCs.

(C) Representative images showing TNT formation and mitochondrial transfer between NMCs and iPSC-MSCs. TNT formation and mitochondrial transfer were partially abrogated by iPSC-MSCs with TNFαIP2 siRNA intervention. (Ci) MITO-GFP-iPSC-MSCs-con^{si} group. (Cii) MITO-GFP-iPSC-MSCs-TNFαIP2^{si} group. (Ciii) Mitochondrial transfer ratio between control siRNA-treated or TNFαIP2 siRNA-treated iPSC-MSCs and NMCs was analyzed by FACS.

(D) (Di) Representative images showing TNT formation by iPSC-MSCs in control, TNF-α, SC-154, or TNF-α + SC-154 group. (Dii) TNT number of one cell in iPSC-MSCs when exposed to TNF-α or TNF-α + SC-514 intervention. (Diii) Western blot showing the level of TNFαIP2, P-P65 NF-κB, and P65 NF-κB in the different groups.

Data represent the means ± SD of three independent experiments. *p < 0.01.
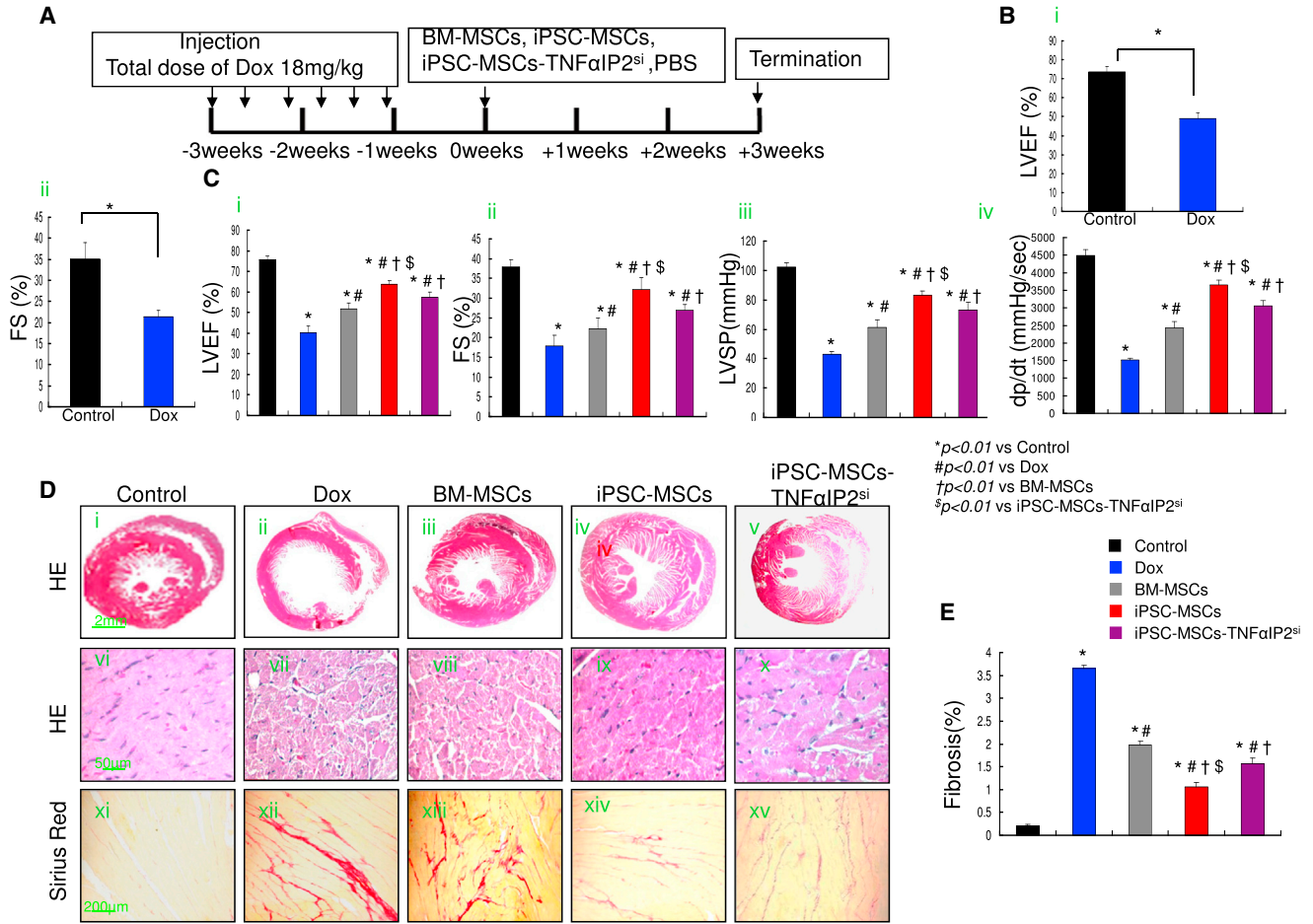
Figure 6. iPSC-MSC Transplantation Attenuates Dox-Induced Cardiomyopathy in Mice

(A) Schematic chart showing the introduction of Dox-induced cardiomyopathy and transplantation of BM-MSCs, iPSC-MSCs, or iPSC-MSCs-TNFαIP2[si].

(B) Heart function, including LVEF and FS, was measured at 0 weeks in control and Dox-treated mice (n = 6 mice per group). Data represent the means ± SD. *p < 0.01.

(C) Effects of BM-MSCs, iPSC-MSCs, and iPSC-MSCs-TNFαIP2[si] on LVEF, FS, and LVSP were assessed at 3 weeks after cell injection (n = 6 mice per group).

(D) At 3 weeks after cell transplantation, histological examination with H&E staining of heart tissue in different groups (Di–Dx). Compared with control mice, a dilated LV cavity and thinner LV walls were observed in Dox-treated mice. Histological sections of heart tissue displayed a different density of cardiomyocyte death, myofibrillar degeneration, and extensive vacuolization among experimental groups (Dvi–Dx). Sirius red staining showed a different degree of myocardium fibrosis among the different experimental groups (Dxi–Dxv).

(E) Quantitative measurement of heart fibrosis in different experimental groups (n = 6 mice per group).

Data represent the means ± SD. *p < 0.01 versus control; #p < 0.01 versus Dox; †p < 0.01 versus BM-MSCs; $p < 0.01 versus iPSC-MSCs-TNFαIP2[si].

transplantation, myocardial fibrosis was significantly reduced compared with the Dox group (Figure 6E). Notably, the extent of myocardial fibrosis in iPSC-MSC-treated mice displayed the most prominent reduction compared with the BM-MSC- or iPSC-MSCs-TNFαIP2[si]-treated group (Figure 6E), suggesting that iPSC-MSCs are superior to BM-MSCs and iPSC-MSCs-TNFαIP2[si] in attenuation of Dox-induced myocardial fibrosis.

iPSC-MSC Attenuated Dox-Induced Cardiomyopathy Is Accompanied by Augmented Mitochondrial Retention and Bioenergetic Reservation

Dox-induced cell apoptosis over the myocardium was largely alleviated after MSC treatment (Figures 7A and 7B). The reduced apoptosis in the iPSC-MSC group was the most distinguished compared with the BM-MSC or iPSC-MSCs-TNFαIP2[si] group (Figure 7B). When we
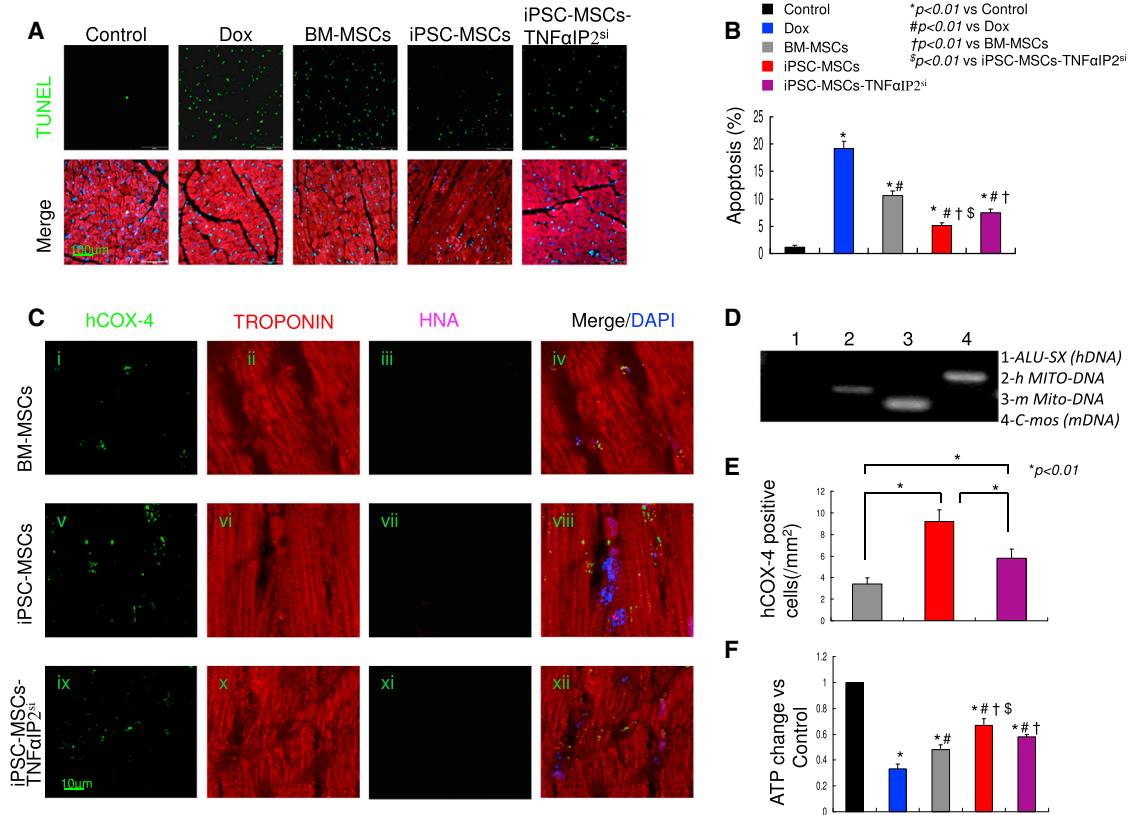
Figure 7. iPSC-MSC Transplantation Ameliorates Dox-Induced Cardiomyopathy and Is Linked to High Mitochondrial Donation and Reserve Mitochondria Functions

(A) At 3 weeks after cell transplantation, apoptosis among the different groups was examined by TUNEL.

(B) Quantitative measurement of the apoptotic rate of the myocardium was expressed as a percentage of positive TUNEL cells versus total DAPI-positive cells per viewing area (n = 6 mice per group).

(C) At 3 weeks after cell transplantation, immunostaining of human COX-4, TROPONIN, and HNA in heart tissue from different experimental groups: BM-MSCs (Ci–Civ), iPSC-MSCs (Civ–Cviii), and iPSC-MSCs-TNFαIP2^{si} (Cix–Cxii).

(D) Mouse heart tissue with human COX-4-positive region was removed by microdissection under a microscope. PCR for *human DNA repeat sequences ALU-SX* (1), *human specific mtDNA* (2), *mouse DNA repeat sequences C-mos* (3), and *mouse specific mtDNA* (4).

(E) Quantitative measurement of COX-4-positive cells of the heart in BM-MSC-, iPSC-MSC-, and iPSC-MSC-TNFαIP2^{si}-treated groups (n = 6 mice per group). Data represent the means ± SD. *p < 0.01.

(F) ATP of heart tissue from different groups. ATP content was expressed as fold change, normalized to the control group (n = 6 mice per group).

Data represent the means ± SD. *p < 0.01 versus control; #p < 0.01 versus Dox; †p < 0.01 versus BM-MSCs; $p < 0.01 versus iPSC-MSCs-TNFαIP2^{si}.

examined human mitochondria in heart tissue harvested 3 weeks after cell transplantation, abundant human mitochondrial protein COX-4 but not human nuclei antigen (HNA) was evident in the mouse TROPONIN-positive CMs, indicating that only human mitochondria from transplanted MSCs were retained in mouse CMs (Figures 7Ci–7Cxii). Mice heart tissue with human COX-4-positive region was isolated by microdissection microscopy. PCR results for human DNA repeat sequences *ALU-SX*, mouse DNA repeat sequences *C-mos* (Lian et al., 2010), *human specific mtDNA*, and *mouse specific mtDNA* (Sokolova et al., 2004) indicated the presence of human mitochondrial genome but no human nuclear genome in the heart tissue (Figure 7D), in agreement with previous studies showing that direct mitochondrial transfer of MSCs plays a key role in tissue repair (Ahmad et al., 2014; Islam et al., 2012; Li et al., 2014). Further, compared with BM-MSC-treated mice, iPSC-MSC-treated mice exhibited far more human COX-4-positive CMs (Figure 7E), suggesting more mitochondria of iPSC-MSCs remained in CMs. Nonetheless, the level of human mitochondrial COX-4 protein in mouse hearts was largely reduced in the

iPSC-MSCs-TNFαIP2[si]-treated mice compared with native iPSC-MSC-treated mice (Figure 7E), in line with in vitro evidence that inhibition of TNFαIP2 attenuated TNF-α-stimulated mitochondrial transfer of iPSC-MSCs.

In addition, Dox-induced reduction of ATP in heart tissue was notably reversed by MSC treatment (Figure 7F). The level of ATP was markedly increased 1.49-fold with iPSC-MSC treatment compared with BM-MSC treatment, whereas this elevation in iPSC-MSCs was markedly abrogated with iPSC-MSCs-TNFαIP2[si] treatment, suggesting that TNFαIP2siRNA-pretreated iPSC-MSCs significantly lose their capacity to rescue Dox-induced mitochondrial damage (Figure 7F).

Increased oxidative stress and excessive inflammation have been considered major mechanisms of Dox-induced cardiomyopathy (Takemura and Fujiwara, 2007). We therefore evaluated the density of dihydroethidium (DHE), 3-nitrotyrosine (3-NT), and malonyldialdehyde (MDA), surrogate markers of oxidative stress. This showed that Dox-increased DHE (Figures S7Ai–S7Avi), 3-NT (Figures S7Bvii–S7Bxii), and MDA (Figure S7Ai) were markedly abrogated by MSC treatment (Figures S7Bvii–S7Bxii), and most prominent in the iPSC-MSC group compared with the BM-MSC and iPSC-MSCs-TNFαIP2[si] groups (Figures S7Avi and S7Bxii). Compared with control mice, Dox-induced mice display severe inflammation as demonstrated by markedly increased accumulation of CD45-positive inflammatory cells (Figures S7Cxiii–S7Cxviii), and, concurrently, elevated levels of pro-inflammatory cytokines MCP-1 and TNF-α in heart tissues (Figures S7Dii and S7Diii). In contrast, MSC transplantation significantly decreased accumulation of CD45-positive cells (Figure S7Cxviii), and reduced the concentration of MCP-1 and TNF-α (Figures S7Dii and S7Diii). Notably, the magnitude of the reduction in CD45-positive cells and the concentration of MCP-1 and TNF-α was most prominent in the iPSC-MSC-treated group compared with the BM-MSC or iPSC-MSCs-TNFαIP2[si] group (Figure S7D).

DISCUSSION

Several reports have shown that BM-MSCs can transfer mitochondria to other cells under various conditions (Cho et al., 2012; Jackson et al., 2016; Spees et al., 2006). Recent results also demonstrate that mitochondrial transfer is an important mechanism of MSC therapy in tissue regeneration (Islam et al., 2012) and repair (Li et al., 2014). The mechanisms of mitochondrial transfer from iPSC-MSCs remain elusive. It has been reported that MIRO1 plays a critical role in the regulation of intercellular mitochondrial transport from MSCs to airway epithelial cells, leading to increased application of MSC-based ther-apy (Ahmad et al., 2014). Our study extends these observations: higher intrinsic MIRO1 in iPSC-MSCs compared with BM-MSCs contributed to higher mitochondrial transfer to NMCs than BM-MSCs. Indeed, inhibition of MIRO1 by shRNA reduced the efficiency of mitochondrial transfer by iPSC-MSCs, whereas overexpression of MIRO1 increased the efficiency.

Emerging evidence suggests that paracrine factor profiling of MSCs is highly dependent on the microenvironment (Gao et al., 2016). Paracrine factors of iPSC-MSCs are reported to effectively rescue Dox-induced CM damage (Zhang et al., 2015). Nevertheless, how the therapeutic efficacy of MSCs is increased in an inflammatory environment has not been well elucidated. Our results revealed crosstalk between the pro-inflammatory microenvironment and the provoked efficiency of mitochondrial transfer from MSCs. Importantly, functional mitochondrial transfer from iPSC-MSCs directly protects CMs against Dox-induced damage. The protection of mitochondrial transfer is separate to the paracrine actions of iPSC-MSCs because CMs without mitochondrial transfer in the same iPSC-MSC co-culture displayed poorer recovery of respiratory dysfunction. Alternatively, when co-culturing iPSC-MSCs and CMs, non-mitochondrial-transferred CMs also exhibited strong resistance to Dox-induced damage, suggesting an important paracrine role of iPSC-MSCs (Zhang et al., 2015). Paracrine action and mitochondrial transfer are two independent but interactive actions that afford MSC-mediated CMs protection against Dox insults. We determined that mitochondrial transfer of iPSC-MSCs can act as a "Trojan horse" through TNF-α induced formation of TNT in vitro. Although the mechanisms remain elusive, a higher level of TNFαIP2 detected in iPSC-MSCs may be responsible for enhanced TNT formation (Hase et al., 2009). We also discovered that a TNF-α/NF-κB/TNFαIP2 signaling pathway is predominantly involved in TNT development for MSC-mediated mitochondrial transfer, indicating that inflammation status may be a critical factor to increase the efficiency of mitochondrial transfer of MSCs, thus enhancing MSC-based therapeutic efficiency. TNF-α activates the NF-κB pathway, which subsequently stimulates TNFαIP2 expression (Chen et al., 2014). Increased TNFαIP2 triggers F-actin polymerization, which may subsequently upregulate TNT formation through actin-driven protrusions of the cytoplasmic membrane in MSCs (Hase et al., 2009; Wang et al., 2011). This contributes to mitochondrial donation from MSCs to NMCs.

The mechanism of the high level of MIRO1 presented in iPSC/ECS-MSCs remains unknown. It has been proposed that compared with the pluripotent stage, during embryonic development, fetal growth, or lineage differentiation of PSCs, increased dynamic mitochondria biogenesis and mobility are needed to meet metabolic shifts for organ

development (Teslaa and Teitell, 2015; Zhang et al., 2011). Indeed, in our databases, we also found that not only MIRO1 but also other molecules involved in mitochondrial network fusion (MFN1 and MFN2) and optic atrophy 1 (OPA1), and mitochondrial mobility MIRO2 and Kif5b, were highly enriched in hESC/iPSC-derived MSC lines. What senses and instructs mitochondrial mass enrichment in lineage-specific MSCs and what other factors facilitate intercellular mitochondrial movement are subjects for future investigation. Whether other mitochondrial motor proteins contribute to intercellular mitochondrial transfer of iPSC-MSCs requires further study. Our results showed that a higher level of intrinsic MIRO1 as well as superior sensitivity to TNF-α-induced TNT formation contribute to the higher mitochondrial transfer potency in iPSC-MSCs. Our study reveals the protective effects of iPSC-MSCs against AIC by efficacious mitochondrial transfer from iPSC-MSCs to injured CMs, independently of MSC paracrine effects, and that augmentation of Dox-induced cardiomyopathy with iPSC-MSCs is attributed to an intrinsically high level of MIRO1 and high sensitivity to TNF-α-induced TNT formation. Our study raises the possibility that modulating mitochondrial transfer by MSCs might be an effective treatment of mitochondrial disorders including AIC.

This study has several limitations. First, our observations are based solely on in vitro and in vivo rodent models. The pathophysiological relevance of our findings should be confirmed in humanoid large animals and clinical studies. Second, although our data demonstrated the obligatory role of MIRO1 and TNT formation in mediating the efficiency of mitochondrial transfer from iPSC-MSCs via TNF-α/NF-kB signaling, the signaling pathways that link other mitochondrial motor proteins involved in intercellular mitochondrial donation need further investigation. Third, although we and others have observed no teratogenic effects of iPSC-MSCs in animal studies (Table S1) (Gruenloh et al., 2011; Lian et al., 2010), the genomic stability of iPSCs needs to be evaluated carefully before their use is translated into clinical practice (Lister et al., 2011). Fourth, the potential role of connexin-43-formed gap junctions (Islam et al., 2012) or microvesicle secretion (Phinney et al., 2015) in mitochondrial transfer has not been investigated in this study.

EXPERIMENTAL PROCEDURE

Cell Culture

Characterized BM-MSCs from healthy adults were commercially acquired from Cambrex BioScience (catalog no. PT-2501). Human iPSC-MSCs derived from iPSC lines were characterized as previously described (Lian et al., 2010). In the current study, two BM-MSCs cell lines and two iPSC-MSCs (Lee NL-iPSC-MSCs and IMR90-iPSC-MSCs) were used. Primary NMCs were obtained and

cultured. HL-1 cells, adult mice CM cell line, and adult human ventricular CM AC16 cells were cultured.

Animal Model

All experiments with live animals were carried out in accordance with relevant guidelines and regulations of the University of Hong Kong and approved by the Committee on the Use of Live Animals in Teaching and Research (CULTAR). A mouse model of AIC was induced in adult mice (6–8 weeks, ICR strain) by intraperitoneal injection of Dox (3 mg/kg, three times per week with a total cumulative dose of Dox of 18 mg/kg) (Zhang et al., 2015). In the negative control group, healthy mice were injected with the same volume of PBS. Echocardiography was performed 1 week after the last Dox injection to confirm the successful creation of an AIC model. Mice with AIC were randomized to receive intramyocardial injection of (1) PBS (Dox group, n = 16), (2) 3.0×10^5 BM-MSCs (BM-MSCs group, n = 14), (3) 3.0×10^5 iPSC-MSCs (iPSC-MSCs group, n = 14), or (4) 3.0×10^5 iPSC-MSCs treated with TNFαIP2siRNA (iPSC-MSCs-TNFαIP2[si] group, n = 12) at four sites in the left ventricle. Three weeks after cell transplantation, hemodynamic measurements were performed after the echocardiographic measurements.

Statistical Analysis

Values are expressed as means ± SD. Significant differences between groups were analyzed by unpaired Student's t test for two groups or one-way ANOVA followed by the Bonferroni test for multiple-group comparison. A p value <0.05 was considered statistically significant.

SUPPLEMENTAL INFORMATION

Supplemental Information includes Supplemental Experimental Procedures, seven figures, one table, and two movies and can be found with this article online at http://dx.doi.org/10.1016/j.stemcr.2016.08.009.

AUTHOR CONTRIBUTIONS

Y.Z., H.-F.T., and Q.L. designed the experiments, analyzed the data, and wrote the manuscript. Y.Z. carried out the experiments with the assistance from D.J., X.L., S.L., Z.Z., W.Y., X.L., S.-M.C., Y.-H.C., Y.L., Y.C., and S.H. A.X. provided the experimental materials. All authors reviewed the manuscript.

ACKNOWLEDGMENTS

REFERENCES

Abounit, S., and Zurzolo, C. (2012). Wiring through tunneling nanotubes - from electrical signals to organelle transfer. J. Cell Sci. *125*, 1089–1098.

Ahmad, T., Mukherjee, S., Pattnaik, B., Kumar, M., Singh, S., Kumar, M., Rehman, R., Tiwari, B.K., Jha, K.A., Barhanpurkar, A.P., et al. (2014). MIRO1 regulates intercellular mitochondrial transport & enhances mesenchymal stem cell rescue efficacy. EMBO J. *33*, 994–1010.

Amsalem, Y., Mardor, Y., Feinberg, M.S., Landa, N., Miller, L., Daniels, D., Ocherashvilli, A., Holbova, R., Yosef, O., Barbash, I.M., et al. (2007). Iron-oxide labeling and outcome of transplanted mesenchymal stem cells in the infarcted myocardium. Circulation *116*, I38–I45.

Arcamone, F., Cassinelli, G., Fantini, G., Grein, A., Orezzi, P., Pol, C., and Spalla, C. (2000). Adriamycin, 14-hydroxydaunomycin, a new antitumor antibiotic from *S. peucetius* var. *caesius*. Reprinted from Biotechnology and Bioengineering, Vol. 11, Issue 6, Pages 1101-1110 (1969). Biotechnol. Bioeng. *67*, 704–713.

Capranico, G., Tinelli, S., and Zunino, F. (1989). Formation, resealing and persistence of DNA breaks produced by 4-demethoxydau-norubicin in P388 leukemia-cells. Chem. Biol. Interact. *72*, 113–123.

Chen, M.H., Colan, S.D., and Diller, L. (2011). Cardiovascular disease: cause of morbidity and mortality in adult survivors of childhood cancers. Circ. Res. *108*, 619–628.

Chen, C.C., Liu, H.P., Chao, M., Liang, Y., Tsang, N.M., Huang, H.Y., Wu, C.C., and Chang, Y.S. (2014). NF-kappaB-mediated transcriptional upregulation of TNFAIP2 by the Epstein-Barr virus oncoprotein, LMP1, promotes cell motility in nasopharyngeal carcinoma. Oncogene *33*, 3648–3659.

Cho, Y.M., Kim, J.H., Kim, M., Park, S.J., Koh, S.H., Ahn, H.S., Kang, G.H., Lee, J.B., Park, K.S., and Lee, H.K. (2012). Mesenchymal stem cells transfer mitochondria to the cells with virtually no mitochondrial function but not with pathogenic mtDNA mutations. PLoS One *7*, e32778.

De Angelis, A., Piegari, E., Cappetta, D., Marino, L., Filippelli, A., Berrino, L., Ferreira-Martins, J., Zheng, H., Hosoda, T., Rota, M., et al. (2010). Anthracycline cardiomyopathy is mediated by depletion of the cardiac stem cell pool and is rescued by restoration of progenitor cell function. Circulation *121*, 276–292.

Gao, F., Chiu, S.M., Motan, D.A., Zhang, Z., Chen, L., Ji, H.L., Tse, H.F., Fu, Q.L., and Lian, Q. (2016). Mesenchymal stem cells and immunomodulation: current status and future prospects. Cell Death Dis. *7*, e2062.

Georgakopoulos, P., Roussou, P., Matsakas, E., Karavidas, A., Anagnostopoulos, N., Marinakis, T., Galanopoulos, A., Georgiakodis, F., Zimeras, S., Kyriakidis, M., et al. (2010). Cardioprotective effect of metoprolol and enalapril in doxorubicin-treated lymphoma patients: a prospective, parallel-group, randomized, controlled study with 36-month follow-up. Am. J. Hematol. *85*, 894–896.

Gruenloh, W., Kambal, A., Sondergaard, C., McGee, J., Nacey, C., Kalomoiris, S., Pepper, K., Olson, S., Fierro, F., and Nolta, J.A. (2011). Characterization and in vivo testing of mesenchymal

stem cells derived from human embryonic stem cells. Tissue Eng. Part A *17*, 1517–1525.

Hase, K., Kimura, S., Takatsu, H., Ohmae, M., Kawano, S., Kitamura, H., Ito, M., Watarai, H., Hazelett, C.C., Yeaman, C., et al. (2009). M-Sec promotes membrane nanotube formation by interacting with Ral and the exocyst complex. Nat. Cell Biol. *11*, 1427–1432.

Holm, C., Stearns, T., and Botstein, D. (1989). DNA topoisomerase II must act at mitosis to prevent nondisjunction and chromosome breakage. Mol. Cell Biol. *9*, 159–168.

Islam, M.N., Das, S.R., Emin, M.T., Wei, M., Sun, L., Westphalen, K., Rowlands, D.J., Quadri, S.K., Bhattacharya, S., and Bhattacharya, J. (2012). Mitochondrial transfer from bone-marrow-derived stromal cells to pulmonary alveoli protects against acute lung injury. Nat. Med. *18*, 759–765.

Jackson, M.V., Morrison, T.J., Doherty, D.F., McAuley, D.F., Matthay, M.A., Kissenpfennig, A., O'Kane, C.M., and Krasnodembskaya, A.D. (2016). Mitochondrial transfer via tunneling nanotubes (TNT) is an important mechanism by which mesenchymal stem cells enhance macrophage phagocytosis in the in vitro and in vivo models of ARDS. Stem Cells *34*, 2210–2223.

Lebrecht, D., Kokkori, A., Ketelsen, U.P., Setzer, B., and Walker, U.A. (2005). Tissue-specific mtDNA lesions and radical-associated mitochondrial dysfunction in human hearts exposed to doxorubicin. J. Pathol. *207*, 436–444.

Lenneman, A.J., Wang, L., Wigger, M., Frangoul, H., Harrell, F.E., Silverstein, C., Sawyer, D.B., and Lenneman, C.G. (2013). Heart transplant survival outcomes for adriamycin-dilated cardiomyopathy. Am. J. Cardiol. *111*, 609–612.

Li, X., Zhang, Y., Yeung, S.C., Liang, Y., Liang, X., Ding, Y., Ip, M.S., Tse, H.F., Mak, J.C., and Lian, Q. (2014). Mitochondrial transfer of induced pluripotent stem cells-derived MSCs to airway epithelial cells attenuates cigarette smoke-induced damage. Am. J. Respir. Cell Mol. Biol. *51*, 455–465.

Lian, Q., Lye, E., Suan Yeo, K., Khia Way Tan, E., Salto-Tellez, M., Liu, T.M., Palanisamy, N., El Oakley, R.M., Lee, E.H., Lim, B., et al. (2007). Derivation of clinically compliant MSCs from CD105+, CD24- differentiated human ESCs. Stem Cells *25*, 425–436.

Lian, Q., Zhang, Y., Zhang, J., Zhang, H.K., Wu, X., Zhang, Y., Lam, F.F., Kang, S., Xia, J.C., Lai, W.H., et al. (2010). Functional mesenchymal stem cells derived from human induced pluripotent stem cells attenuate limb ischemia in mice. Circulation *121*, 1113–1123.

Lister, R., Pelizzola, M., Kida, Y.S., Hawkins, R.D., Nery, J.R., Hon, G., Antosiewicz-Bourget, J., O'Malley, R., Castanon, R., Klugman, S., et al. (2011). Hotspots of aberrant epigenomic reprogramming in human induced pluripotent stem cells. Nature *471*, 68–73.

Phinney, D.G., Di Giuseppe, M., Njah, J., Sala, E., Shiva, S., St Croix, C.M., Stolz, D.B., Watkins, S.C., Di, Y.P., Leikauf, G.D., et al. (2015). Mesenchymal stem cells use extracellular vesicles to outsource mitophagy and shuttle microRNAs. Nat. Commun. *6*, 8472.

Pinarli, F.A., Turan, N.N., Pinarli, F.G., Okur, A., Sonmez, D., Ulus, T., Oguz, A., Karadeniz, C., and Delibasi, T. (2013). Resveratrol and adipose-derived mesenchymal stem cells are effective in the

prevention and treatment of doxorubicin cardiotoxicity in rats. Pediatr. Hematol. Oncol. *30*, 226–238.

Sokolova, V.A., Kustova, M.E., Arbuzova, N.I., Sorokin, A.V., Moskaliova, O.S., Bass, M.G., and Vasilyev, V.B. (2004). Obtaining mice that carry human mitochondrial DNA transmitted to the progeny. Mol. Reprod. Dev. *68*, 299–307.

Spees, J.L., Olson, S.D., Whitney, M.J., and Prockop, D.J. (2006). Mitochondrial transfer between cells can rescue aerobic respiration. Proc. Natl. Acad. Sci. USA *103*, 1283–1288.

Suliman, H.B., Carraway, M.S., Ali, A.S., Reynolds, C.M., Welty-Wolf, K.E., and Piantadosi, C.A. (2007). The CO/HO system reverses inhibition of mitochondrial biogenesis and prevents murine doxorubicin cardiomyopathy. J. Clin. Invest. *117*, 3730–3741.

Sun, Y.Q., Zhang, Y., Li, X., Deng, M.X., Gao, W.X., Yao, Y., Chiu, S.M., Liang, X., Gao, F., Chan, C.W., et al. (2015). Insensitivity of human iPS cells-derived mesenchymal stem cells to interferon-gamma-induced HLA expression potentiates repair efficiency of hind limb ischemia in immune humanized NOD Scid gamma mice. Stem Cells *33*, 3452–3467.

Takemura, G., and Fujiwara, H. (2007). Doxorubicin-induced cardiomyopathy from the cardiotoxic mechanisms to management. Prog. Cardiovasc. Dis. *49*, 330–352.

Teslaa, T., and Teitell, M.A. (2015). Pluripotent stem cell energy metabolism: an update. EMBO J. *34*, 138–153.

Vallabhaneni, K.C., Haller, H., and Dumler, I. (2012). Vascular smooth muscle cells initiate proliferation of mesenchymal stem cells by mitochondrial transfer via tunneling nanotubes. Stem Cells Dev. *21*, 3104–3113.

Wang, Y., Cui, J., Sun, X., and Zhang, Y. (2011). Tunneling-nanotube development in astrocytes depends on p53 activation. Cell Death Differ. *18*, 732–742.

Xin, Y., Wang, Y.M., Zhang, H., Li, J., Wang, W., Wei, Y.J., and Hu, S.S. (2010). Aging adversely impacts biological properties of human bone marrow-derived mesenchymal stem cells: implications for tissue engineering heart valve construction. Artif. Organs *34*, 215–222.

Zhang, J., Khvorostov, I., Hong, J.S., Oktay, Y., Vergnes, L., Nuebel, E., Wahjudi, P.N., Setoguchi, K., Wang, G., Do, A., et al. (2011). UCP2 regulates energy metabolism and differentiation potential of human pluripotent stem cells. EMBO J. *30*, 4860–4873.

Zhang, Y., Liang, X., Liao, S., Wang, W., Wang, J., Li, X., Ding, Y., Liang, Y., Gao, F., Yang, M., et al. (2015). Potent paracrine effects of human induced pluripotent stem cell-derived mesenchymal stem cells attenuate doxorubicin-induced cardiomyopathy. Sci. Rep. *5*, 11235.